Two-dimensional numerical computation of the structure-dependent spectral response in a 4H-SiC metal–semiconductor–metal ultraviolet photodetector with consideration of reflection and absorption on contact electrodes*

Chen Bin(陈斌)†, Yang Yintang(杨银堂), Chai Changchun(柴常春), Song Kun(宋坤), and Ma Zhenyang(马振洋)

Key Laboratory of Ministry of Education for Wide Band-Gap Semiconductor Materials and Devices, School of Microelectronics, Xidian University, Xi'an 710071, China

Abstract: A two-dimensional model of a 4H-SiC metal–semiconductor–metal (MSM) ultraviolet photodetector has been established using a self-consistent numerical calculation method. The structure-dependent spectral response of a 4H-SiC MSM detector is calculated by solving Poisson's equation, the current continuity equation and the current density equation. The calculated results are verified with experimental data. With consideration of the reflection and absorption on the metal contacts, a detailed study involving various electrode heights (H), spacings (S) and widths (W) reveals conclusive results in device design. The mechanisms responsible for variations of responsivity with those parameters are analyzed. The findings show that responsivity is inversely proportional to electrode height and is enhanced with an increase of electrode spacing and width. In addition, the ultraviolet (UV)-to-visible rejection ratio is $> 10^3$. By optimizing the device structure at 10 V bias, a responsivity as high as 180.056 mA/W, a comparable quantum efficiency of 77.93% and a maximum UV-to-visible rejection ratio of 1875 are achieved with a detector size of $H = 50$ nm, $S = 9$ μm and $W = 3$ μm.

Key words: MSM structure; ultraviolet photodetector; spectral response
DOI: 10.1088/1674-4926/32/8/084001 **PACC:** 0670D; 0762; 7820

1. Introduction

Over the last decade, ultraviolet (UV) detection has been of great interest for a wide range of commercial and military applications, particularly in areas such as ozone layer monitoring, intersatellite/underwater communications, flame detection, emitter calibration, chemical and biological analysis, UV-astrophysics, high-speed optoelectronic integrated circuit connection and sampling, UV dosage detection and spectrum measurement[1−3]. With the recent advance in SiC material growth and processing, 4H-SiC photodetectors have become promising candidates for UV detection due to their excellent physical and electronic properties, such as a very low dark current, a significantly higher operating temperature and insensibility to visible/IR background. A great deal of effort has been devoted to proposing and fabricating various types of detectors, including Schottky diodes[4, 5], p–n photodiodes[6], p–i–n photodiodes[7, 8] and metal–semiconductor–metal diodes[9−11]. Compared to these structures, MSM UV detectors may be superior due to their large device bandwidth, ultralow intrinsic capacitance and a fabrication process that is compatible with field effect transistors. However, MSM photodetectors still suffer from low responsivity due to optical losses on the electrode and spacing in the opaque metal contacts. Extensive work have been focused on improving the bandwidth-efficiency product, time response and dark/illuminated current–voltage characteristics[12−14]. To date, no systematic investigation has been carried out on responsivity versus structure parameters with consideration of the reflection and absorption on metal electrodes. Therefore, it is significant to design an appropriate device structure for responsivity enhancement.

In this paper, a numerical model of a 4H-SiC MSM photodetector is presented with a two-dimensional (2D) device simulator ISE-DESSIS. Based on the model, MSM UV detectors with various structural parameters are simulated in order to demonstrate whether their structure-dependent responsivity is consistent with our expectation. Then, the responsivity characteristics are discussed in detail and structural optimization is employed to achieve outstanding performance.

2. Methodology

2.1. Device structure and parameters

A schematic diagram of the 4H-SiC MSM photodetector used in our calculation is illustrated in Fig. 1. The device em-

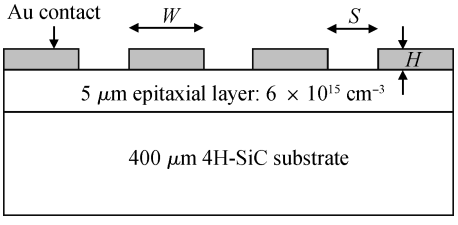

Fig. 1. Schematic cross section of a 4H-SiC MSM UV detector.

* Project supported by the Pre-Research Foundation from the National Ministries and Commissions (Nos. 51323040118, 513080302).
† Corresponding author. Email: xidianchenbin@163.com
Received 24 February 2011, revised manuscript received 1 April 2011
© 2011 Chinese Institute of Electronics

Table 1. Summary of bandgap structure parameters (BSP) and incomplete ionization parameters (IIP) used in the calculation[16].

Parameter	Value
E_g	3.26 eV
E_{g0}	3.359 eV
α	3.3×10^{-4} eV/K
β	0 K
T	300 K
E_ND	0.065 eV
alpha_N	3.1×10^{-8} eV·cm
g_ND	2
Xsec_N	1×10^{-12} cm^2/s
NdCrit	1×10^{22} cm^{-3}

ploys two Schottky contacts on top of an epitaxial layer to form a planar interdigital structure. It consists, starting from the top, of an Au contact electrode (due to its high work function), a 5 μm epitaxial layer with a doping concentration of 6×10^{15} cm^{-3} and a 400 μm 4H-SiC substrate with a doping concentration of 10^{20} cm^{-3}, respectively. The height of the contact electrode is 80 nm. The fingers are 3 μm wide and 500 μm long with a spacing of 3 μm. The optical sensitive area of the detector is 200×500 μm^2. For meaningful comparison, the calculated device structure is similar to the fabricated detector previously reported in Ref. [15].

2.2. Numerical modeling

A typical MSM photodetector is comprised of two Schottky contacts connected back to back. Under an applied voltage, one of the contacts is forward biased and the other is reverse biased. Unlike a p–n junction detector, the MSM photodetector is basically a majority carrier only device. When UV light illuminates the active area, the carriers are generated in the bulk material and swept by the built-in field of Schottky contacts. The special MSM structure accounts for an inherent low capacitance and a faster response. Due to the outstanding properties of wide bandgap materials, the 4H-SiC MSM photodetector is suitable for UV detection. Compared to silicon, 4H-SiC has wide bandgap and the impurities are not completely ionized at room temperature. The key differences are considered in the device simulation. The 4H-SiC bandgap and incomplete ionization parameters are summarized in Table 1. To investigate the 4H-SiC MSM UV detector, numerical modeling is realized using a 2D simulator DESSIS, which computes electric potential and carrier distribution by iteratively solving the Poisson equation and the current-continuity equations. In addition, the different physical models used simultaneously in DESSIS are the mobility model, the Shockley–Read–Hall (SRH) recombination model, the thermionic emission model, the barrier lowering model and the optical generation model. The doping dependent mobility can be characterized using the Masetti model[16]. The model is expressed as

$$\mu_{\rm dop} = \mu_{\rm min1} \exp\left(-\frac{p_{\rm c}}{N_{\rm i}}\right) + \frac{\mu_{\rm const} - \mu_{\rm min2}}{1 + \left(\dfrac{N_{\rm i}}{C_{\rm r}}\right)^{\alpha}} - \frac{\mu_1}{1 + \left(\dfrac{C_{\rm s}}{N_{\rm i}}\right)^{\beta}}, \tag{1}$$

where $N_{\rm i}$ denotes the total concentration of ionized impurities and $\mu_{\rm const}$ is determined by the constant mobility model[16]. $\mu_{\rm min1}$, $\mu_{\rm min2}$ and μ_1 , as well as the reference doping concentrations $P_{\rm c}$, $C_{\rm r}$ and $C_{\rm s}$ and the exponents α and β are specified in Ref. [16].

The recombination in the course of photo-generated carrier transportation is described by the SRH model[16], which is given by

$$R_{\rm net}^{\rm SRH} = \frac{np - n_{\rm i,\,eff}^2}{\tau_{\rm p}(n + n_1) + \tau_{\rm n}(p + p_1)}, \tag{2}$$

$$n_1 = n_{\rm i,\,eff} \exp\frac{E_{\rm trap}}{kT}, \tag{3}$$

$$p_1 = n_{\rm i,\,eff} \exp\left(-\frac{E_{\rm trap}}{kT}\right), \tag{4}$$

where $E_{\rm trap}$ is the difference between the defect level and the intrinsic level. $n_{\rm i,\,eff}$ denotes the effective intrinsic density. The minority lifetimes, $\tau_{\rm n}$ and $\tau_{\rm p}$, are modeled as a product of a doping dependent $\tau_{\rm dop}$, a field dependent $g_{\rm c}(f)$ and a temperature dependent factor $f(T)$. Lifetimes are written as

$$\tau_{\rm c} = \tau_{\rm dop}\left\{f(T)/[1 + g_{\rm c}(f)]\right\}, \quad {\rm c} = {\rm n, p}, \tag{5}$$

where c = n or c = p for electrons or holes. In our calculation, thermionic emission is critical for determining the proper device characteristics due to its description of the hetero-junction interface between the metal and the semiconductor[16]. The model is expressed as

$$J_{\rm n,\,2} = aq\left[v_{\rm n,\,2}n_2 - \frac{m_2}{m_1}v_{\rm n,\,1}n_1 \exp\left(-\frac{\Delta E_{\rm c}}{K_{\rm B}T_{\rm e,\,1}}\right)\right], \tag{6}$$

where $a = 2$, $J_{\rm n,\,2}$ is the electron current density entering the metal and $J_{\rm n,\,1}$ is the electron current density leaving the semiconductor. Then $J_{\rm n,\,2}$ is equal to $J_{\rm n,\,1}$. The emission velocities are defined as

$$v_{\rm n,\,i} = \sqrt{K_{\rm B}T_{\rm e,\,i}/2\pi m_{\rm i}}, \tag{7}$$

where $i = 1$ or 2 for the semiconductor or the metal. In order to match realistic results, it is essential to consider the barrier lowering model in order to explain the effect of barrier lowering caused by image force. The barrier lowering model can be applied to a Schottky contact[16]. The following expression is used to compute the value of the barrier lowering.

$$\Delta\phi_{\rm B}(E) = a_1\left[\left(\frac{E}{E_0}\right)^{p_1} - \left(\frac{E_{\rm eq}}{E_0}\right)^{p_1}\right] + a_2\left[\left(\frac{E}{E_0}\right)^{p_2} - \left(\frac{E_{\rm eq}}{E_0}\right)^{p_2}\right], \tag{8}$$

where E is the absolute value of the electric field, $E_0 = 1$, $E_{\rm eq}$ is the equilibrium electric field that is used to have $\Delta\phi_{\rm B} = 0$ at the equilibrium and a_1, a_2, p_1, p_2 are model coefficients specified in the DESSIS parameter file. To numerically calculate the photocurrent, an accurate optical model is needed. In our calculation, the input UV optical signal is supported by ISE-DESSIS via multiple vertical photon beams. The photon beams affect the net photon flux that reaches the device surface and are related to optical generation rate[16], which is given by

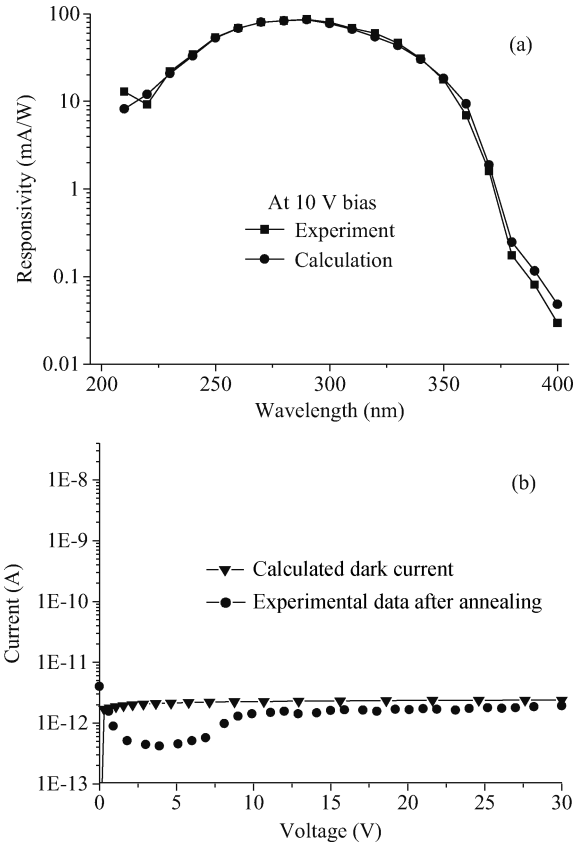

Fig. 2. Comparison of (a) the calculated responsivity and (b) dark current–voltage characteristics of a 3 μm finger width and spacing 4H-SiC MSM detector with experimental data[15].

$$G^{\text{opt}}(z,t) = J_0 F_{\text{t}}(t) F_{\text{xyv}} \alpha(\lambda, z') \exp\left(-\left|\int_{Z_0}^{Z} \alpha(\lambda, z')\mathrm{d}z'\right|\right), \tag{9}$$

where J_0 denotes the incident beam intensity. $F_{\text{t}}(t)$ is the beam time behavior function. F_{xyv} is equal to one inside the semiconductor and decreases to zero outside the semiconductor. Z_0 is the coordinate of the semiconductor surface. To describe the optical characteristics of a 4H-SiC MSM UV detector, several key input optical parameters including WavePower $= 2.5 \times 10^{-4}$ (W/cm^2), Wavelength $= 2.1 \times 10^{-5} - 4 \times 10^{-5}$ (cm), SemAbs $= \alpha$ (cm^{-1}) and SemWindows $= (0, 2 \times 10^{-2})$ (cm) are also considered in the calculation, which specify incident wave power, the wavelength, a constant value α for absorption coefficient obtained from the published data in Ref. [17] and the optical window for the 2D case, respectively.

3. Results and discussion

3.1. Verification of the numerical model

Spectral responsivity is one of the most important characteristics of UV detector, which can be calculated using

$$R = \frac{\displaystyle\int_0^L Q\frac{P}{h\nu}\eta\alpha(1-r)\exp(-\alpha x)\mathrm{d}x}{P_{\text{opt}}}, \tag{10}$$

where P and P_{opt} are the input optical power and effective absorption optical power, r is the reflection coefficient, Q is the photon-generated charge and η denotes the quantum efficiency closely related to the device parameters. Based on the above models and a self-consistent solution of the Poisson and electron/hole continuity equations, the simulator DESSIS is used to calculate the spectral response of a 4H-SiC MSM UV detector with a numerical coupling algorithm and appropriate boundary conditions on a 2D mesh. With the same device structure as a realistic detector, the calculated responsivity result is illustrated in Fig. 2(a). For comparison, the experimental UV spectral responsivity is also shown. It can be seen that the calculated and experimental results are in good agreement. Without an optical model, the dark current–voltage characteristics can be obtained. The calculation results and the experimental data are shown in Fig. 2(b). It is clear that the calculated and measured data are around 2 pA, especially when the applied voltages are higher than 9 V. For bias voltages lower than 9 V, the calculated result is somewhat larger than the measured curve due to an idealization of the numerical model. However, a relatively good agreement between the calculated and measured characteristics of responsivity and dark current is achieved, which validates the numerical model in this study.

3.2. Influence of the device structure on responsivity

To investigate the impact of structural parameters on the responsivity of the photodetector, we firstly take the contact height into consideration. In theory, the responsivity of an MSM detector is correlated to the expression.

$$R = \frac{\lambda}{1.24}\eta_{\text{i}}(1-r)\frac{s}{s+w}[1-\exp(-\alpha d)], \tag{11}$$

with λ being the wavelength in micrometers, η_{i} expressing the internal quantum efficiency, the term $1-r$ accounting for Fresnel losses and d denoting thickness of the active layer. According to Eq. (11), it is noted that the spectral response has noting to do with electrode height. In fact, when UV illumination occurs on the surface of the detector, the UV beams can be reflected and absorbed by the contact electrodes. Indeed, some UV light will penetrate the electrodes in order to produce photon-generation carriers. Therefore, electrode height may exert a strong influence on the responsivity of the detector. In our calculation, we obtain the reflection coefficient r of Au film in Ref. [18] and extract the absorption coefficient α of a Au finger electrode by

$$I = I_0(1-r)\exp(-\alpha d). \tag{12}$$

Here I/I_0 denotes the transmittance and d is the electrode height, which have been given from transmittance spectra in Ref. [3]. Then, we can calculate the optical transmittance of various thicknesses of Au electrodes. Based on the consideration above, the spectral response is calculated with a series of electrode heights ranging from 20 to 200 nm, plotted in Fig. 3. As is shown, we find that the responsivity gradually decreases with the increase of contact height. The inset of Fig. 3 illustrates the enlarged spectral response versus contact height, which indicates that responsivity is inversely proportional to electrode height. Specifically, under 10 V bias and 300 nm illumination, it should be noted from the inset that the responsivity is around 75.1 mA/W when the contact height increases

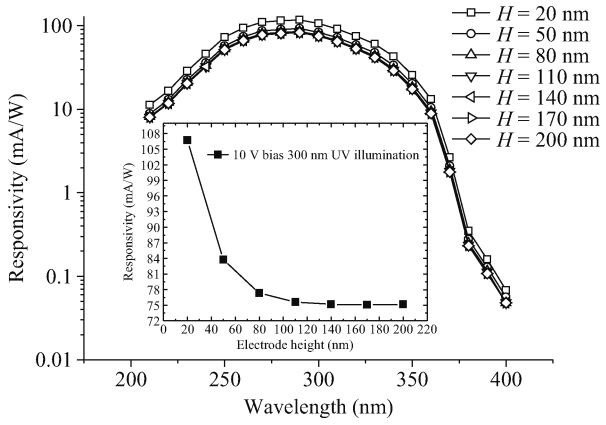

Fig. 3. Influence of various electrode heights on the spectral response of a 4H-SiC MSM photodetector. Inset shows the enlarged responsivity as a function of contact height at the illumination wavelength of 300 nm and 10 V bias.

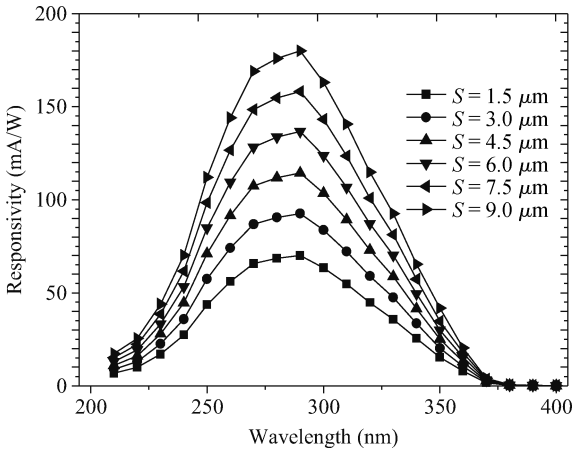

Fig. 4. Photoresponse of a 4H-SiC MSM photodetector with a 50 nm electrode height, 3 μm contact width and various finger spacings at 10 V bias.

from 140 to 200 nm and then drastically increases from 75.604 to 106.724 mA/W as the height decreases from 110 to 20 nm. These results are probably due to the fact that UV transparency increases with a thinner metal electrode, leading to more UV light impinging on the active region under the contact electrodes. It is also clear that the variations of responsivity are nearly a constant in the spectra region between 370 and 400 nm. Obvious changes of response versus contact height are observed in the region ranging from 280 to 320 nm.

We find that the peak responsivity occurs at 290 nm for various contact heights. The maximum and minimum responsivities at 290 nm are 117.94 and 82.892 mA/W, corresponding to the quantum efficiency of 50.43% and 35.44% with electrode heights of 20 nm and 200 nm, respectively. A point to note is that responsivity can be improved by decreasing the height of the contact, owing to the exponential increase of transparency of the thinner metal electrode. Hence, the lower the electrode height is, the higher the UV transmittance will be and, in turn, the spectral response for the detector is enhanced. However, an electrode height of around 20 nm can cause concerns about the uniformity of an ultra-thin Schottky barrier and can also be a detrimental factor for the mechanical and thermal stability of the contact[19]. Therefore, a reasonable electrode height of 50 nm is desirable for the following calculation and analysis of the 4H-SiC MSM UV detector.

Figure 4 shows the spectral response of a 4H-SiC MSM photodetector with 50 nm electrode height, 3 μm electrode width and diverse finger spacings at 10 V bias, revealing a strong dependence of responsivity on geometry sizes. Not only can we see that the peak responsivity increases with the increase of finger spacing, but also the remarkable changes of other points on the curves as compared to the family of response curves shown in Fig. 3. It is found that the responsivity ranges are broad, from 220 to 380 nm, and do not exhibit an abrupt spectral cutoff due to the fact that 4H-SiC is an indirect semiconductor and does not have a sharp cutoff edge at the band edge. Therefore, the long wavelength cutoff edge occurs at 380 nm because of the band-gap of 4H-SiC, while the short wavelength cutoff is ascribed to the larger photo carrier recombination in the short wavelength region. The peak zone

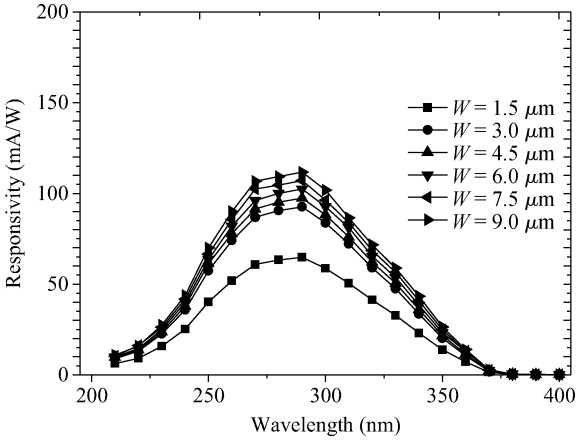

Fig. 5. Responsivity of 4H-SiC MSM photodetector with various electrode widths at a bias of 10 V while finger height and spacing remain 50 nm and 3 μm, respectively.

is located around 290 nm. As shown in Fig. 4, it is clear that the peak spectral response increases distinctly from 70.08 to 180.056 mA/W, when the metal finger spacing increases from 1.5 to 9 μm. The influence of electrode spacing on the photoresponse is most likely due to the photosensitive area dependence of the MSM UV detector. The photosensitive area is proportional to finger spacing. As the electrode spacing increases, more UV incident light will illuminate and be absorbed onto photosensitive area, which will produce more photon-generated carriers under UV illumination. Such a change of illumination area has a slight influence on the SRH recombination rate. Hence, they may account for the increase of spectral response.

The electrode width dependence of responsivity for a 50 nm contact height, 3 μm-spacing 4H-SiC MSM detector is illustrated in Fig. 5. As depicted, the responsivity rises continuously for an increasing metal contact width from 1.5 to 9 μm. A similar tendency but for a different spectral response can be seen in Figs. 4 and 5, indicating that responsivity enhances with an increase of metal electrode spacing and width. For the latter, the increment of photoresponse in all wavelengths of interest

is less than the former. An analogous increase of photocurrent with larger finger width can be found in Ref. [20], which substantiates the calculated trend. As is clearly visible in Fig. 5, the curves are almost all closely arranged, except for the one with a relatively narrow electrode width of 1.5 μm. In the UV region of 240 to 360 nm, not only can notable changes be observed, but also the overall responsivity is enhanced as electrode width increases. Taking into account the UV transmittance in the electrode, the improvement of responsivity may be attributed to the increase of finger width, since wider and thinner contacts can effectively increase the incident area and thus increase the number of photo-generated carriers. The maximal responsivity obtained at 290 nm are 102.404, 107.06 and 111.763 mA/W for three detectors with contact widths of 6, 7.5 and 9 μm, respectively, lower than the relevant peak values of 136.748, 158.244 and 180.056 mA/W in Fig. 4 with finger spacing instead. Therefore, the variation of electrode spacing has a more significant influence on responsivity.

3.3. Analysis and optimization

By changing electrode spacing and width, we can find an improvement in the characteristics of responsivity illustrated in Figs. 4 and 5, revealing that electrode spacing and width are two factors affecting the spectral response of the detector but with different working mechanisms. For the former, we ascribe it to the increase of photosensitive area.

When the bias is low, the thin depletion layer is not beneficial for lower-energy photons to be absorbed in order to generate photocurrent. As the applied voltage increases further, the incomplete depletion region extends rapidly and becomes entirely reverse biased. With the electric field around, the photoelectrons drift towards the electrodes and the thicker depletion layer facilitates their collection. As the carriers reach the active region, the responsivity of the MSM UV detector will be higher with a larger photosensitive area. For the latter, the cause is due to the increase of the effective transmittance area under the electrodes. A tentative explanation is presented as follows. It is concluded that the wider finger contact possesses a larger current density than the narrow one illustrated in Fig. 6. Clearly, the distribution of current density is inhomogeneous at the edges of the electrodes, demonstrating that the current density around the edges of the contacts is larger than in the central region of the electrodes. Similar behavior and analysis are available in Ref. [21]. When the finger width increases, the electric field becomes more extensive and thus accelerates the charge accumulation at the edges of the contacts. With UV illumination, the increasing bias induces an increase in current owing to Schottky barrier lowering caused by charge accumulation at the edges of the metal–semiconductor interface. Simultaneously, the reverse bias could cause an increase of band bending near the edge of the Schottky contact[22]. Consequently, with the increase of finger widths, the effect of charge inhomogeneous accumulation at the edges of contacts is amplified, thus improving the photoelectron collection. In addition, the electric field under the contact electrode decays greatly with an increase of vertical depth. The degraded electric field limits the mobility velocity of photon-generation carriers. The wider the contact width is, the more extensive the vertical electrical distribution will be. With UV illumination of the active

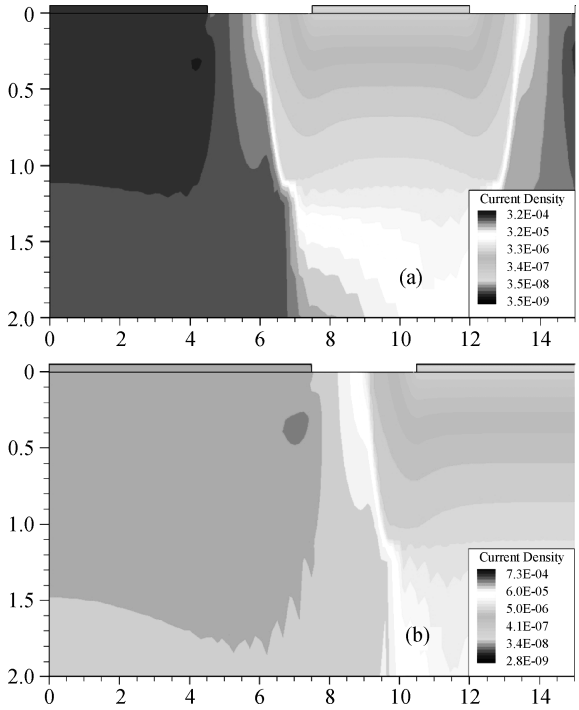

Fig. 6. TECPLOT calculation of the cross-sectional current density distribution for 3 μm spacing MSM photodetectors with different electrode widths of (a) 4.5 μm and (b) 7.5 μm under 290 nm UV illumination and 30 V applied voltage.

region, photon-generated carriers are separated and promptly swept between the electrodes before recombination by an extensive electric field. Thus, a noticeably large photocurrent is obtained. From a design point of view, the structure of an MSM photodetector depends on three parameters, not only the electrode height (H), but also the width (W) and spacing (S). The influences of the latter two factors on device performance are more remarkable. A detector with wider spacing and width possesses a spacious UV absorption area and a more extensive vertical electrical field distribution. However, problems such as device noise characteristics and a delay of response time are inevitable. Specifically, the large finger spacing increases the carrier transport distance and hence the transit time. Moreover, the increasing electrode width may result in the degradation of noise characteristics due to the increase of dark current. Therefore, a tradeoff between the electrode width and spacing should be taken into account comprehensively. In the calculation, we optimize the values of H, W and S to pursue better performance in terms of a high UV-to-visible rejection ratio and comparable quantum efficiency.

Here, we define the UV-to-visible rejection ratio as the responsivity calculated at 290 nm divided by the responsivity calculated at 400 nm. With such a definition and a 10 V applied bias, it is concluded that the UV-to-visible contrast ratios are around three orders of magnitude for all the geometrical parameters illustrated in Fig. 7. The variation of UV-to-visible contrast ratio ranges from 1273 to 1875 with the structural parameters of $W = 9$ μm, $S = 3$ μm and $W = 3$ μm, $S = 9$ μm, respectively. It is found that the ratio decreases with an increase of electrode width. The detector with a 9 μm electrode width and 3 μm spacing possesses the maximum re-

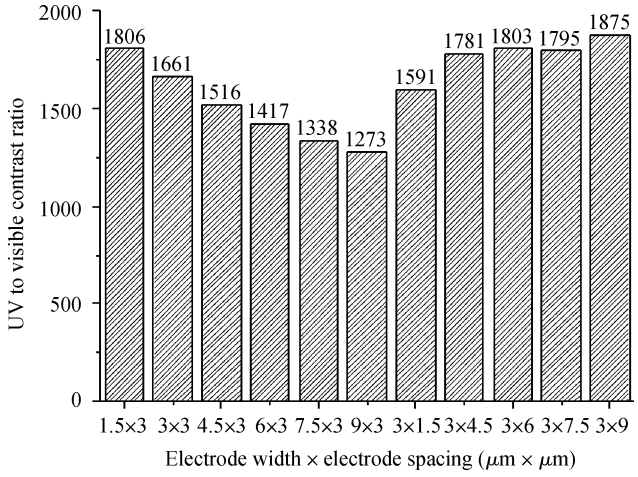

Fig. 7. UV-to-visible rejection ratios of MSM photodetectors with a 50 nm electrode height and various device structures.

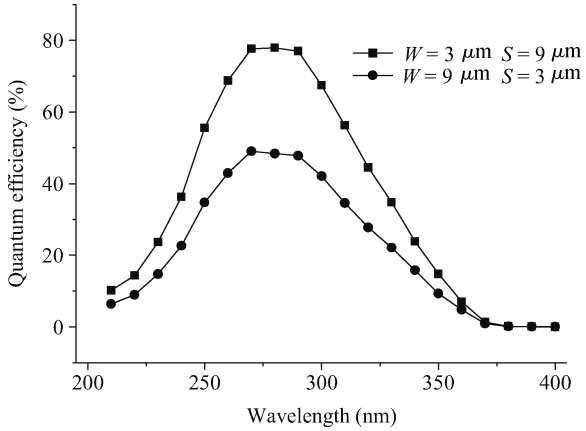

Fig. 8. Calculated quantum efficiency versus wavelength for two 4H-SiC MSM photodetectors with 50 nm electrode height and different device structures at 10 V applied bias.

sponsivity in Fig. 5. In contrast, its UV-to-visible contrast is undesirable due to its lower responsivity at 400 nm. Furthermore, the quantum efficiency of two MSM photodetectors is presented in Fig. 8, which is regarded as another crucial characteristic of the detector and can be expressed as $\eta = 1241R/\lambda$. It is clear that quantum efficiency works as a function of wavelength. The peak zones of quantum efficiency are located at 270 to 300 nm for both detectors. Then, the two curves drop with the increasing wavelength to 380 nm. The penetration depth ($1/\alpha$) around 380 nm is about 625 μm, larger than the thickness of the device's active area. When 380 nm UV light illuminates the detector, it will penetrate the optical sensitive area. Such a low efficiency to form a photocurrent is mainly attributed to the lower absorption coefficient of around 400 nm. With the same wavelength ranges of 210 to 400 nm, the quantum efficiency increases gradually from 0.027% to 49.031% and from 0.03% to 77.93% for two photodetectors with geometry sizes of $W = 9$ μm, $S = 3$ μm and $W = 3$ μm, $S = 9$ μm. Therefore, the latter is the optimum choice for UV detection due to the increase of the visible-blind rejection ratio and peak quantum efficiency, of 47.29% and 61.11%, respectively.

4. Conclusions

We have established a model of a 4H-SiC MSM UV detector using a numerical calculation method. The validity of our present model has been confirmed with experimental data. By considering the UV transmittance of a metal electrode, a systematic investigation of the structural dependency of responsivity in an MSM UV detector is carried out in order to obtain better performance. The findings show that electrode height has a direct influence on the spectral response of the detector, indicating that the lower the height of the electrode is, the higher the spectral response will be. In contrast, the impacts of electrode spacing and width on responsivity are more considerable. We find that all of the rejection ratios are around three orders of magnitude for diverse device structures. Finally, the maximum responsivity, peak quantum efficiency and outstanding UV-to-visible contrast of 180.056 mA/W, 77.93% and 1875 are achieved for a detector with 50 nm electrode height, 3 μm width and 9 μm spacing, which is an excellent performance for UV detection.

References

[1] Zhang Y G, Li A Z, Milnes A G. Metal–semiconductor–metal ultraviolet photodetectors using 6H-SiC. IEEE Photonics Technol Lett, 1997, 9(3): 363

[2] Yang W F, Zhang F, Liu Z G, et al. High responsivity 4H-SiC based metal–semiconductor–metal ultraviolet photodetectors. Sci China Ser G Phys Mech Astron, 2008, 51(11): 1616

[3] Su Y K, Chang S J, Chen C H, et al. GaN metal–semiconductor–metal ultraviolet sensors with various contact electrodes. IEEE Sensors J, 2002, 2(4): 366

[4] Chang S J, Lee K H, Chang P C, et al. AlGaN/GaN Schottky barrier photodetector with multi-Mg_xN_y/GaN buffer. IEEE Sensors J, 2009, 9(2): 87

[5] Hu J, Xin X B, Zhao J H, et al. Highly sensitive visible-blind extreme ultraviolet Ni/4H-SiC Schottky photodiodes with large detection area. Opt Lett, 2006, 31(11): 1591

[6] Chuah L S, Hassan Z, Abu Hassan H, et al. P-GaN/n-Si heterojunction photodiodes. Surf Rev Lett, 2008, 15(5): 699

[7] Zhang Y, Shen S C, Kim H J, et al. Low-noise GaN ultraviolet p–i–n photodiodes on GaN substrates. Appl Phys Lett, 2009, 94(22): 221109

[8] Afzalian A, Flandre D. Physical modeling and design of thin-film SOI lateral PIN photodiodes. IEEE Trans Electron Devices, 2005, 52(6): 1116

[9] Li J, Zhao M, Wang X F. High performance Schottky UV photodetectors based on epitaxial AlGaN thin film. Physica B, 2010, 405(3): 996

[10] Wang L X, Chen X K, Wu G, et al. Study on trapping center and trapping effect in MSM ultraviolet photo-detector on microcrystalline diamond film. Phys Status Solidi A, 2010, 207(2): 468

[11] Chen M R, Chang S H, Chen T C, et al. Fabrication study of AlN solar-blind (< 280 nm) MSM photodetectors grown by low-temperature deposition. Phys Status Solidi A, 2010, 207(1): 224

[12] Kato K. Ultrawide-band/high-frequency photodetectors. IEEE Trans Microw Theory Tech, 1999, 47(7): 1265

[13] Zhao X, Currie M, Cola A, et al. Time response of two-dimensional gas-based vertical field metal–semiconductor–metal photodetectors. IEEE Trans Electron Devices, 2008, 55(7): 1762

[14] Chen B, Yang Y T, Li Y J, et al. Simulation and optimization of a 6H-SiC metal–semiconductor–metal ultraviolet photodetector.

J Semicond, 2010, 31(6): 064010
[15] Yang W F, Zhang F, Liu Z G, et al. Effects of annealing on the performance of 4H-SiC metal–semiconductor–metal ultraviolet photodetectors. Mater Sci Semicond Process, 2008, 11(2): 59
[16] DESSIS, 2D Semiconductor Device Simulator version 10.0 2005 Integrated Systems Engineering, Zurich
[17] Sridhara S G, Devaty R P, Choyke W J. Absorption coefficient of 4H silicon carbide from 3900 to 3250 Å. J Appl Phys, 1998, 84(5): 2963
[18] Dmitruk N L, Fursenko O V, Kondratenko O S, et al. Optical characteristization of thin Au films by standard and polaritonic ellipsometry. Semicond Phys Quantum Electron Optoelectron, 2003, 6(3): 349
[19] Sciuto A, Roccaforte F, Di Franco S, et al. High efficiency 4H-SiC Schottky UV-photodiodes using self-aligned semitransparent contacts. Superlattices Microstruct, 2007, 41(1): 29
[20] Zhang J Q, Yang Y T, Lou L F, et al. Current–voltage characteristics simulation and analysis of 4H-SiC metal–semiconductor–metal ultraviolet photodetectors. Chin Opt Lett, 2008, 6(8): 615
[21] Zhao D G, Jiang D S, Liu Z S, et al. An anomalous gain mechanism in GaN Schottky barrier ultraviolet photodetectors. Chin Phys Lett, 2009, 26(5): 058501
[22] Sabuktagin S, Moon Y T, Dogan S, et al. Observation of surface charging at the edge of a Schottky contact. IEEE Electron Device Lett, 2006, 27(4): 211